Supplement of Nat. Hazards Earth Syst. Sci., 18, 2047–2056, 2018
https://doi.org/10.5194/nhess-18-2047-2018-supplement

Natural Hazards and Earth System Sciences
Open Access
EGU

Supplement of

Changing seasonality of moderate and extreme precipitation events in the Alps

Stefan Brönnimann et al.

Correspondence to: Stefan Brönnimann (stefan.broennimann@giub.unibe.ch)

Supplementary Material

Table S1: COREDX model simulations and modeling groups (CLMcom - CLM Community, HMS - Hungarian Meteorological Service, ICTP - International Centre for Theoretical Physics, ICHE - Irish Centre for High-End Computing, MPI - Max Planck Institute for Meteorology, SMHI - Swedish Meteorological and Hydrological Institute, KNMI - Royal Netherlands Meteorological Institute, IPSL - Institut Pierre-Simon-Laplace, DMI - Danish Meteorological Institute, CNRM - National Centre for Meteorological Research, MOHC - UK Met Office, Hadley Center).

Ensemble	Regional Model	Global Model	Member
CORDEX11, RCP8.5	CLMcom.CCLM4.8.17	CNRM.CERFACS.CNRM.CM5	r1i1p1
	CLMcom.CCLM4.8.17	ICHEC.EC.EARTH	r12i1p1
	CLMcom.CCLM4.8.17	MOHC.HadGEM2.ES	r1i1p1
	CLMcom.CCLM4.8.17	MPI.M.MPI.ESM.LR	r1i1p1
	CNRM.ALADIN53	CNRM.CERFACS.CNRM.CM5	r1i1p1
	DMI.HIRHAM5	ICHEC.EC.EARTH	r3i1p1
	IPSL.INERIS.WRF331F	IPSL.IPSL.CM5A.MR	r1i1p1
	KNMI.RACMO22E	ICHEC.EC.EARTH	r1i1p1
	MPI.CSC.REMO2009	MPI.M.MPI.ESM.LR	r1i1p1
	MPI.CSC.REMO2009	MPI.M.MPI.ESM.LR	r2i1p1
	SMHI.RCA4	CNRM.CERFACS.CNRM.CM5	r1i1p1
	SMHI.RCA4	ICHEC.EC.EARTH	r12i1p1
	SMHI.RCA4	IPSL.IPSL.CM5A.MR	r1i1p1
	SMHI.RCA4	MOHC.HadGEM2.ES	r1i1p1
	SMHI.RCA4	MPI.M.MPI.ESM.LR	r1i1p1
CORDEX44, RCP8.5	CLMcom.CCLM4.8.17	MPI.M.MPI.ESM.LR	r1i1p1
	CNRM.ALADIN53	CNRM.CERFACS.CNRM.CM5	r1i1p1
	DMI.HIRHAM5	ICHEC.EC.EARTH	r3i1p1
	HMS.ALADIN52	CNRM.CERFACS.CNRM.CM5	r1i1p1
	ICTP.RegCM4.3	MOHC.HadGEM2.ES	r1i1p1
	IPSL.INERIS.WRF331F	IPSL.IPSL.CM5A.MR	r1i1p1
	KNMI.RACMO22E	ICHEC.EC.EARTH	r1i1p1
	MPI.CSC.REMO2009	MPI.M.MPI.ESM.LR	r1i1p1
	MPI.CSC.REMO2009	MPI.M.MPI.ESM.LR	r2i1p1
	SMHI.RCA4	CCCma.CanESM2	r1i1p1
	SMHI.RCA4	CNRM.CERFACS.CNRM.CM5	r1i1p1
	SMHI.RCA4	CSIRO.QCCCE.CSIRO.Mk3.6.0	r1i1p1
	SMHI.RCA4	ICHEC.EC.EARTH	r12i1p1
	SMHI.RCA4	IPSL.IPSL.CM5A.MR	r12i1p1

	SMHI.RCA4	MIROC.MIROC5	r1i1p1
	SMHI.RCA4	MOHC.HadGEM2.ES	r1i1p1
	SMHI.RCA4	MPI.M.MPI.ESM.LR	r1i1p1
	SMHI.RCA4	NCC.NorESM1.M	r1i1p1
	SMHI.RCA4	NOAA.GFDL.GFDL.ESM2M	r1i1p1
CORDEX11, RCP4.5	CLMcom.CCLM4.8.17	CNRM.CERFACS.CNRM.CM5	r1i1p1
	CLMcom.CCLM4.8.17	ICHEC.EC.EARTH	r12i1p1
	CLMcom.CCLM4.8.17	MOHC.HadGEM2.ES	r1i1p1
	CLMcom.CCLM4.8.17	MPI.M.MPI.ESM.LR	r1i1p1
	CNRM.ALADIN53	CNRM.CERFACS.CNRM.CM5	r1i1p1
	DMI.HIRHAM5	ICHEC.EC.EARTH	r3i1p1
	IPSL.INERIS.WRF331F	IPSL.IPSL.CM5A.MR	r1i1p1
	KNMI.RACMO22E	ICHEC.EC.EARTH	r1i1p1
	MPI.CSC.REMO2009	MPI.M.MPI.ESM.LR	r1i1p1
	MPI.CSC.REMO2009	MPI.M.MPI.ESM.LR	r2i1p1
	SMHI.RCA4	CNRM.CERFACS.CNRM.CM5	r1i1p1
	SMHI.RCA4	ICHEC.EC.EARTH	r12i1p1
	SMHI.RCA4	IPSL.IPSL.CM5A.MR	r1i1p1
	SMHI.RCA4	MOHC.HadGEM2.ES	r1i1p1
	SMHI.RCA4	MPI.M.MPI.ESM.LR	r1i1p1
CORDEX44, RCP4.5	CLMcom.CCLM4.8.17	MPI.M.MPI.ESM.LR	r1i1p1
	CNRM.ALADIN53	CNRM.CERFACS.CNRM.CM5	r1i1p1
	DMI.HIRHAM5	ICHEC.EC.EARTH	r3i1p1
	IPSL.INERIS.WRF331F	IPSL.IPSL.CM5A.MR	r1i1p1
	KNMI.RACMO22E	ICHEC.EC.EARTH	r1i1p1
	MPI.CSC.REMO2009	MPI.M.MPI.ESM.LR	r1i1p1
	MPI.CSC.REMO2009	MPI.M.MPI.ESM.LR	r2i1p1
	SMHI.RCA4	CCCma.CanESM2	r1i1p1
	SMHI.RCA4	CNRM.CERFACS.CNRM.CM5	r1i1p1
	SMHI.RCA4	CSIRO.QCCCE.CSIRO.Mk3.6.0	r1i1p1
	SMHI.RCA4	ICHEC.EC.EARTH	r12i1p1
	SMHI.RCA4	IPSL.IPSL.CM5A.MR	r12i1p1
	SMHI.RCA4	MIROC.MIROC5	r1i1p1
	SMHI.RCA4	MOHC.HadGEM2.ES	r1i1p1
	SMHI.RCA4	MPI.M.MPI.ESM.LR	r1i1p1
	SMHI.RCA4	NCC.NorESM1.M	r1i1p1
	SMHI.RCA4	NOAA.GFDL.GFDL.ESM2M	r1i1p1

17

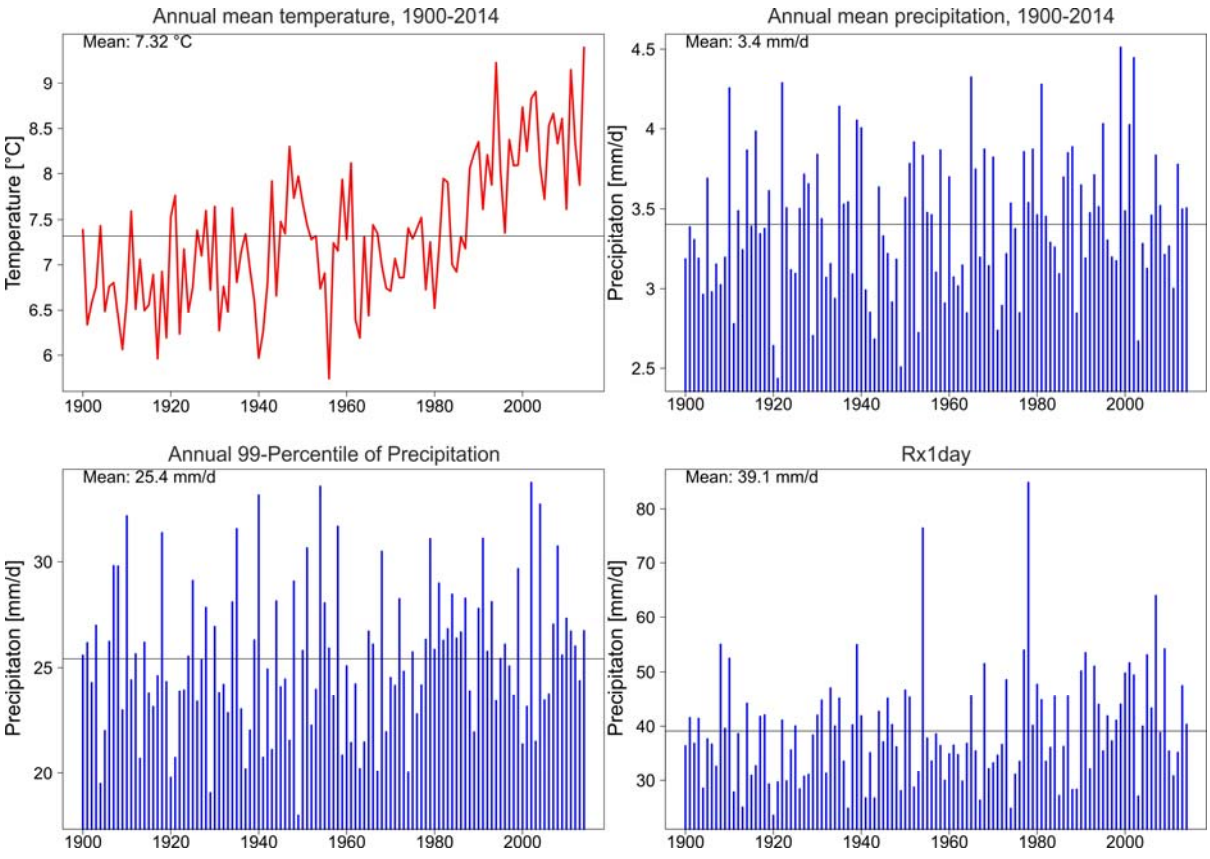

Fig. S1: Catchment-averaged temperature and precipitation statistics based on the average of the stations shown in Fig. 1. Shown are mean temperature, mean precipitation, the annual 99th percentile of precipitation and Rx1day for the period 1900–2014.

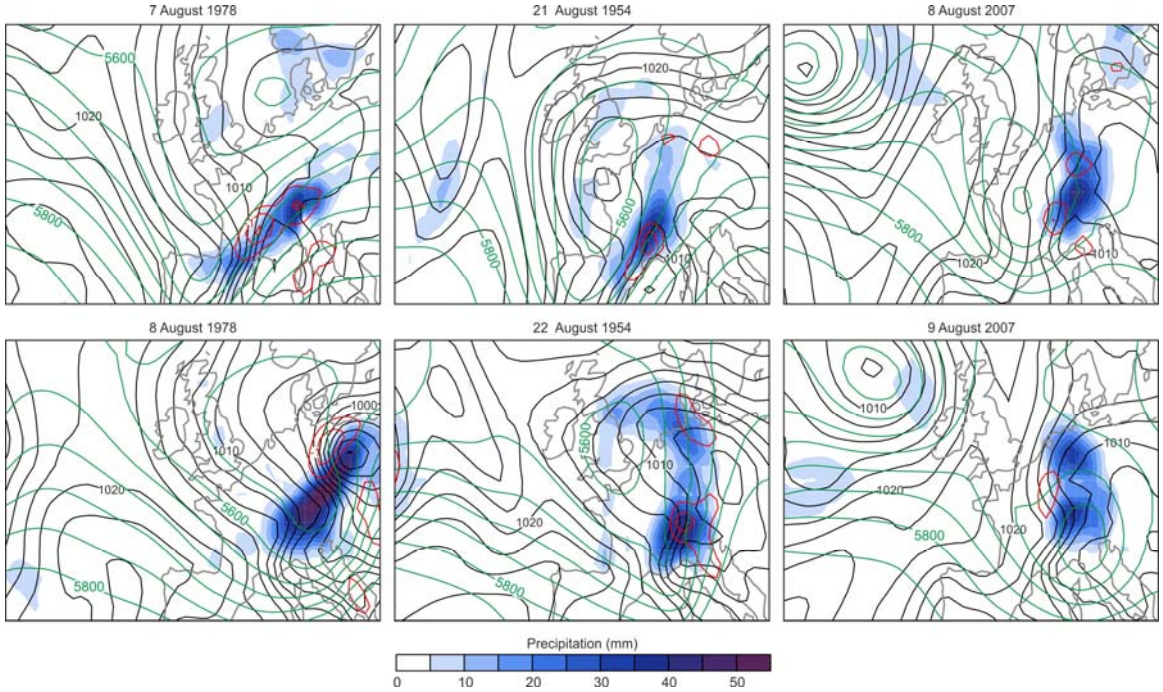

Fig. S2: Reanalysis fields of sea-level pressure (in hPa, black contour), 500 hPa geopotential height (green, in gpm), omega at 500 hPa (in Pa s^{-1}, only upward motion shown) and precipitation from CERA-20C for the largest three Rx1day events in the catchment-averaged observations (see Table 2).

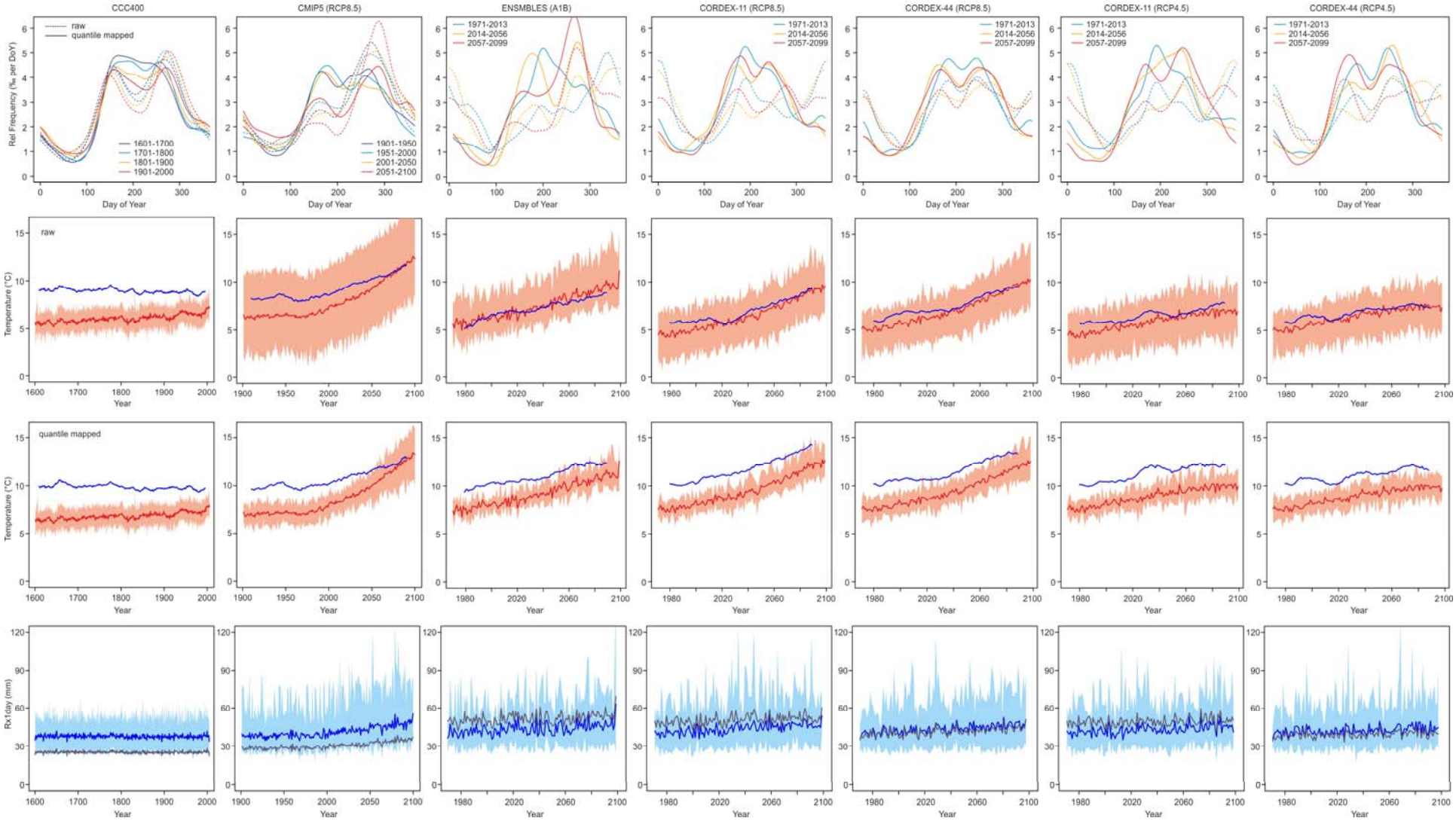

Fig. S3: Difference between raw and quantile mapped data for CCC400, CMIP5, ENSEMBLES, CORDEX-11 and CORDEX44 (both RCP4.5 and RCP8.5). (from top to bottom) Day of occurrence of Rx1day for different periods, annual mean temperature and temperature during Rx1day events, and Rx1day (ensemble mean as line and ensemble range as shading; grey line in bottom row indicates the raw data).

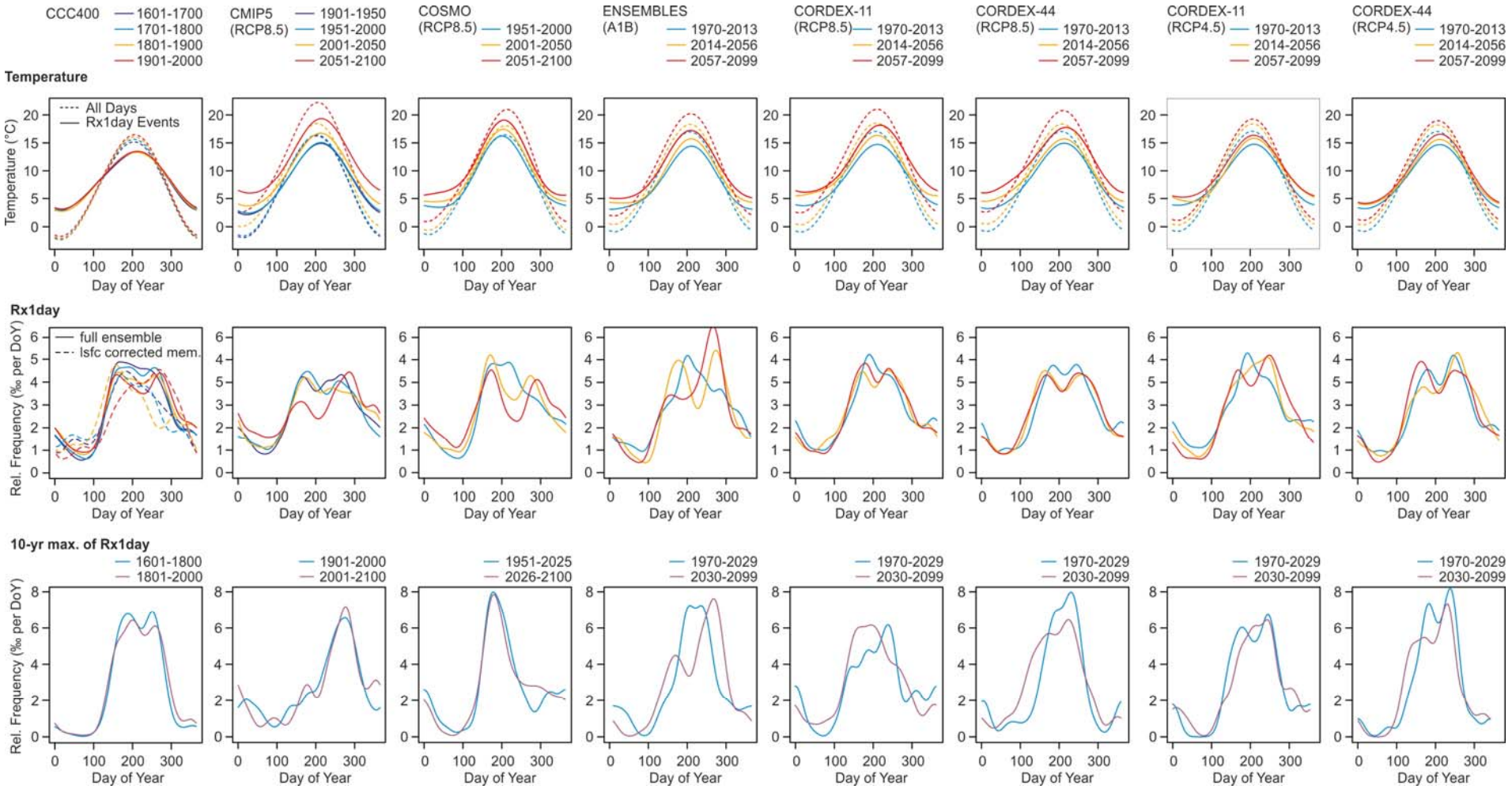

Fig. S4: (top row) Annual mean temperature for all days and for Rx1day (obtained by fitting the first two harmonics of the annual cycle) for the CCC400, CMIP5 and COSMO ensembles for different time periods. (second row) Density plot of the day of occurrence of Rx1day events for different time periods. (bottom row) Same as second row, but only for the highest Rx1day per decade. Note that instead of using 100-yr (CCC400) or 50-yr periods, the period length is increased to 200 yrs for CCC400, 100 yrs for CMIP and 75 yrs for COSMO. All analyses are based on quantile-mapped data. A Gaussian Kernel smoother with a bandwidth of 15 days was used for plotting. For CCC400 we also show a density plot for single member with corrected land surface (with a bandwidth of 25 days).

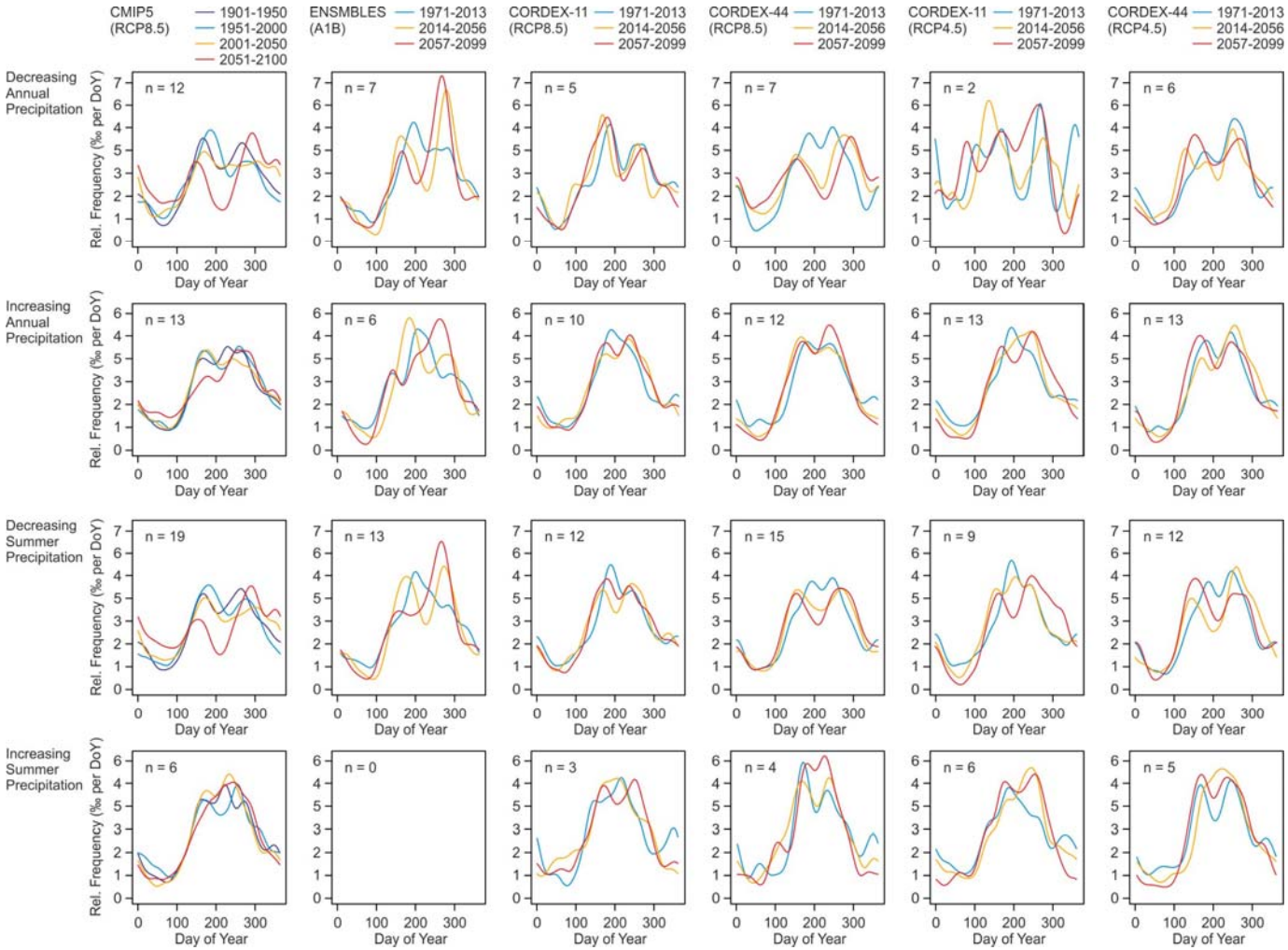

Fig. S5: Density plot of the day of occurrence of Rx1day for different time periods in the multi-model ensembles CMIP5 (same periods as in Fig. S3) as well as in ENSEMBLES, CORDEX-11, and CORDEX-44 (each split into three subperiods). The ensemble members are separated into those that show a positive or negative trend in annual mean or summer mean precipitation over the entire time period (*n* indicates the number of simulations per case, multiplying this number with the period length yields the number of data points on which each plot is based). A Gaussian Kernel smoother with a bandwidth of 15 days was used for plotting.

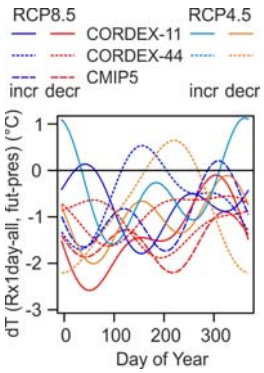

Fig. S6: Temperature difference as a function of calendar day between event days (Rx1day) and all days, expressed as difference between the future (2065–2099) and the present (1971–2005). The plot is the same as in Fig. 3 (top right), but with the simulations stratified into those with increasing or decreasing summer precipitation (only multi-model ensembles; ENSEMBLES is not shown as all members show decreased summer precipitation).

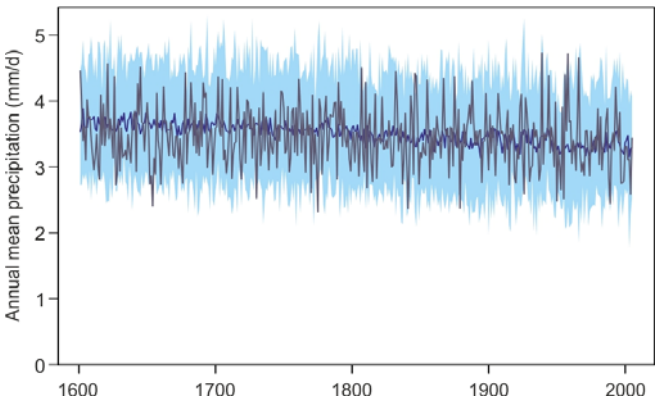

Fig. S7: Annual mean precipitation in CCC400. Solid blue line and shading indicate ensemble mean and range, the grayish line shows the run with corrected land-surface.